G. Ghirardo[1]

Ansaldo Energia Switzerland,
Römerstrasse 36,
Baden 5401, Switzerland
e-mail: giulio.ghirardo@ansaldoenergia.com

C. Di Giovine

Ansaldo Energia Switzerland,
Römerstrasse 36,
Baden 5401, Switzerland

J. P. Moeck

Institut für Strömungsmechanik und
Technische Akustik,
Technische Universität Berlin,
Berlin 10623, Germany;
Department of Energy and
Process Engineering,
Norwegian University of Science and
Technology,
Trondheim 7491, Norway

M. R. Bothien

Ansaldo Energia Switzerland,
Römerstrasse 36,
Baden 5401, Switzerland

Thermoacoustics of Can-Annular Combustors

Can-annular combustors consist of a set of independent cans, connected on the upstream side to the combustor plenum and on the downstream side to the turbine inlet, where a transition duct links the round geometry of each can with the annular segment of the turbine inlet. Each transition duct is open on the sides toward the adjacent transition ducts, so that neighboring cans are acoustically connected through a so-called cross-talk open area. This theoretical, numerical, and experimental work discusses the effect that this communication has on the thermoacoustic frequencies of the combustor. We show how this communication gives rise to axial and azimuthal modes, and that these correspond to particularly synchronized states of axial thermoacoustic oscillations in each individual can. We show that these combustors typically show clusters of thermoacoustic modes with very close frequencies and that a slight loss of rotational symmetry, e.g., a different acoustic response of certain cans, can lead to mode localization. We corroborate the predictions of azimuthal modes, clusters of eigenmodes, and mode localization with experimental evidence. [DOI: 10.1115/1.4040743]

Introduction

Can-annular combustors are common in heavy-duty land based gas turbines. In this design, the air flows from the compressor outlet to the combustor plenum. From there, the air stream splits into N cans. Each can consists of a first approximation of a cylinder that is connected upstream to the plenum and of one or more fuel injector(s) and respective combustion zone(s) [1]. After the last combustion zone, the hot gas flows into the turbine inlet. Since the can cross section is circular and the inlet of the turbine is an annular gap, a special transition duct is designed to suitably link the two, as sketched in Fig. 1.

High frequency thermoacoustic instabilities are localized in the regions close to the flame. As such, they are not specific of annular or can-annular types of combustors. We focus instead on low frequency thermoacoustic instabilities, i.e., on frequencies below the cut-on frequency of transversal modes in each can. While thermoacoustic modes in annular combustors have received ample attention over the last decade [2–5], the same is not true for can-annular systems. Krebs et al. [6] show that low frequency acoustic modes are axial in each can, but particular attention is required when one considers the acoustics in the N transition ducts, both because of their complex geometry and because of the acoustic communication occurring between adjacent transition ducts. Land-based can-annular gas turbines have an even number N of cans because of the common design of the combustor casing, which comprises an upper and a lower part with a horizontal flange inbetween. An odd number of cans would require fixing a can at the flange location. We then consider in the following the case of N even, but the methods and the results are rather similar for the case of N odd, which is more common in aero-derivative engines [7]. Kaufmann et al. [8] discuss how thermoacoustic mode shapes differ between a single-can test rig and a model of a quarter of an engine comprising four cans. More recently, Farisco and coworkers have studied the acoustic cross-talk communication between neighboring cans [9–12]. We show in this paper that

the low frequency modes have certain peculiar features in can-annular combustors that are related to this cross-talk communication.

The Effect of Asymmetry section of the paper discusses the effect of asymmetries in can-annular combustors. This has been investigated for annular combustors by various groups (for example, Refs. [2], [4], and [13–16]); however, to our knowledge, these aspects have not been addressed yet for can-annular configurations. Although both types of systems feature the same nominal symmetry—a discrete rotational symmetry—a qualitatively different response to asymmetries can be expected. This is associated with the relatively weak coupling between the individual cans. In the present work, we will study asymmetry effects based on an elementary network model for a can-annular system, with a realistic transfer matrix for the can-to-can coupling at the turbine inlet.

The Rotationally Symmetric Case

In this section, we assume that all cans are the same, i.e., that the system has rotational and reflection symmetry. Typically, the geometry of the cans is the same for all the cans, and the preferential clockwise or anticlockwise direction of the mean flow as it enters the turbine stator plays a role in a part of the acoustic domain that is acoustically compact in comparison with the wavelength of interest. We will discuss later the effect of the loss of this rotational symmetry.

Because of the rotational symmetry, according to Bloch theory [14,17], the solutions in the frequency domain of the acoustic pressure field $\hat{p}$ in the N cans can be written in the form

$$\hat{p}(\boldsymbol{x}) = \psi(\boldsymbol{x})e^{im\theta}, \quad m = -N/2 + 1, \dots, 0, 1, \dots, N/2 \quad (1)$$

where θ is the azimuthal coordinate around the axis of discrete rotational symmetry, the turbine rotor, and $\psi(\boldsymbol{x})$ is periodic in θ with period $2\pi/N$ (i.e., ψ is identical in all cans). The nth can is centered at the azimuthal position

$$\theta_n = (n-1)\frac{2\pi}{N} \quad (2)$$
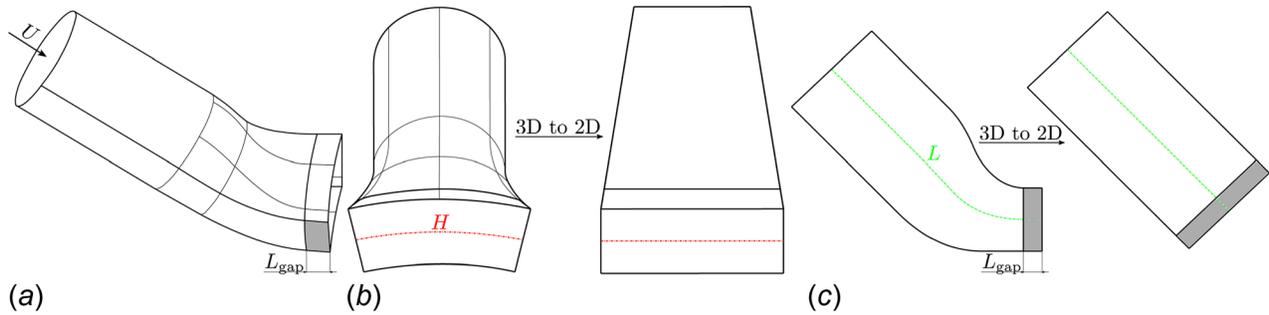
Fig. 1 Geometry of a typical transition duct and the simplifications leading to the two-dimensional (2D) model, appearing ultimately in Fig. 2(a). The communicating gap between two adjacent transition ducts is colored in gray, with an axial length L_{gap}. (a) three-dimensional (3D) sketch of a transition duct, (b) front view of the air volume, and (c) side view of the air volume.

in a frame of reference where the first can is at the origin. In Eq. (1), the integer m is called the Bloch wavenumber, and in our application, it is the azimuthal order of the solution, because in time domain the solution $p(x,t) = \hat{p}(x)e^{i\omega t} = \psi(x)e^{i(\omega t + m\theta)}$ is a spinning[2] wave in the azimuthal coordinate θ. For example, $m = \pm 2$ denote two counter-rotating spinning waves of azimuthal order 2. All these modes appear in counter-rotating, degenerate pairs, except for the mode $m = N/2$ and $m = 0$ that are nondegenerate and are considered next.

In particular, for $m = 0$ we obtain an axial mode, while for $m = N/2$ we observe from Eq. (1) that the solution in the nth can is

$$\hat{p}_n(x) = \psi(x)e^{i\frac{N}{2}(n-1)\frac{2\pi}{N}} = \psi(x)e^{i(n-1)\pi} = (-1)^{n-1}\psi(x) \quad (3)$$

From Eq. (3), it follows that the solution for $m = N/2$ changes sign from one can to the next, i.e., the acoustic field of one can is in anti-phase with respect to the acoustic field of its two neighboring cans. For this reason, the mode $m = N/2$ is called a push-pull mode, in analogy with the change of sign.

One can look for solutions for a fixed value of m by studying the solution ψ in Eq. (1) in one can only, by applying Bloch boundary conditions at the interface between two neighboring cans, i.e., at the two side zones with length L_{gap} in Figs. 1(a) and 1(c). This is discussed in the Transition Ducts' Modeling section. From the study of one can for all possible values of m, one can calculate the response of all the cans accounting for all azimuthal modes.

Transition Ducts' Modeling. The Mach number is low in the transition duct main cross section, typically below 0.2. We then neglect low-Mach number effects in the volume and assume a zero mean flow in the wave equation. From upstream to downstream, the cross section of a transition duct goes from circular to approximately rectangular, as sketched in Fig. 1(a). In particular, it broadens on the sides and it thins in the orthogonal direction as presented in Figs. 1(b) and 1(c). This leads to an overall modest change of the cross section area. Moreover, the axial progression of this area change is particularly smooth because it is designed to avoid flow separation. One can then study the effect of the slowly varying cross section on the acoustics [18–20]. Because this change of the cross section is modest and depends strongly on the specific combustor, it is neglected in the following. We also neglect the curvature upstream of the turbine inlet presented with the center green line in Fig. 1(c) and neglect also the slight turn in the azimuthal direction, as presented with the red line in Fig. 1(b). This leads to the bidimensional, rectangular domain of Fig. 2(a). The small effect of these geometrical approximations will be validated later by comparing the results obtained on the exact 3D geometry of a set of $N = 12$ real transition ducts and on their 2D equivalent counterpart.

We focus instead on the cross-talk area where acoustic communication between transition ducts occurs, colored in gray in Fig. 1, with an axial length L_{gap}.

We choose two nondimensional numbers describing the geometry. The first is the aspect ratio L/H of the 2D domain in Fig. 2(a). The second is the ratio L_{gap}/H, which can be interpreted as the strength of the can-to-can communication. The reference values for the two numbers are presented in Table 1. When we later investigate the effect of one nondimensional number, we keep the other constant.

The Helmholtz number of the stator $He_s = L_s\omega/c$ is typically low for axial modes in heavy-duty gas turbines at the turbine inlet, where ω is the acoustic angular frequency of interest and c is the speed of sound. This means that the first stator length L_s can be assumed as acoustically compact as compared to the acoustic wavelength $2\pi c/\omega$ of interest. Moreover, the Mach number is high at the turbine inlet so that we can model the acoustic response of the turbine inlet with a reflection coefficient with a fixed gain <1 and a zero phase response[3] [22]. Since the focus is not on the turbine inlet reflection, we fix a reflection coefficient gain equal to unity, i.e., apply homogeneous Neumann boundary conditions for the pressure field on the downstream end of the domain in Fig. 2(a), and expect only a small quantitative effect when accounting for a gain lower than 1, as found for example by Bauerheim et al. [23]. We also neglect from the study the occurrence of entropy wave generation from the flame and their reflection at the turbine inlet [24] and references therein], assuming that it plays a negligible role. The discussed modeling simplifications lead to the bidimensional domain of the transition duct presented in Fig. 2(a). On the black and red contours, we apply homogeneous Neumann boundary conditions, and on the blue contour, Bloch boundary conditions

$$\psi(x, H/2) = \psi(x, -H/2)e^{i\frac{2\pi}{N}m} \quad x \in [L - L_{gap}, L] \quad (4)$$

where m is the azimuthal wavenumber and the domain spans a distance H in the vertical direction in Fig. 2(a). The Helmholtz equation is solved by discretizing the 2D domain on Chebyshev nodes and expressing the solution as a truncated Chebyshev series [25]. This spectral solution allows a very quick numerical calculation of the eigensolutions and in turn very quick sensitivity studies on the governing parameters. The spectral solver has been verified against a commercial finite element method solver.

Modes' Shapes and Cans' Synchronization. In this section, we fix a number $N = 14$ of cans, present the theoretical results, and validate them with engine data. We discuss the axial mode $m = 0$, the push–pull mode $m = N/2 = 7$, and the second azimuthal mode $m = 2$, in this order. The considerations that apply to the

---

[2]That is traveling in the azimuthal direction at the speed of sound.

[3]One can account for finite Helmholtz number effects by extending the axial domain by an equivalent end length correction [21], affecting only slightly the results.
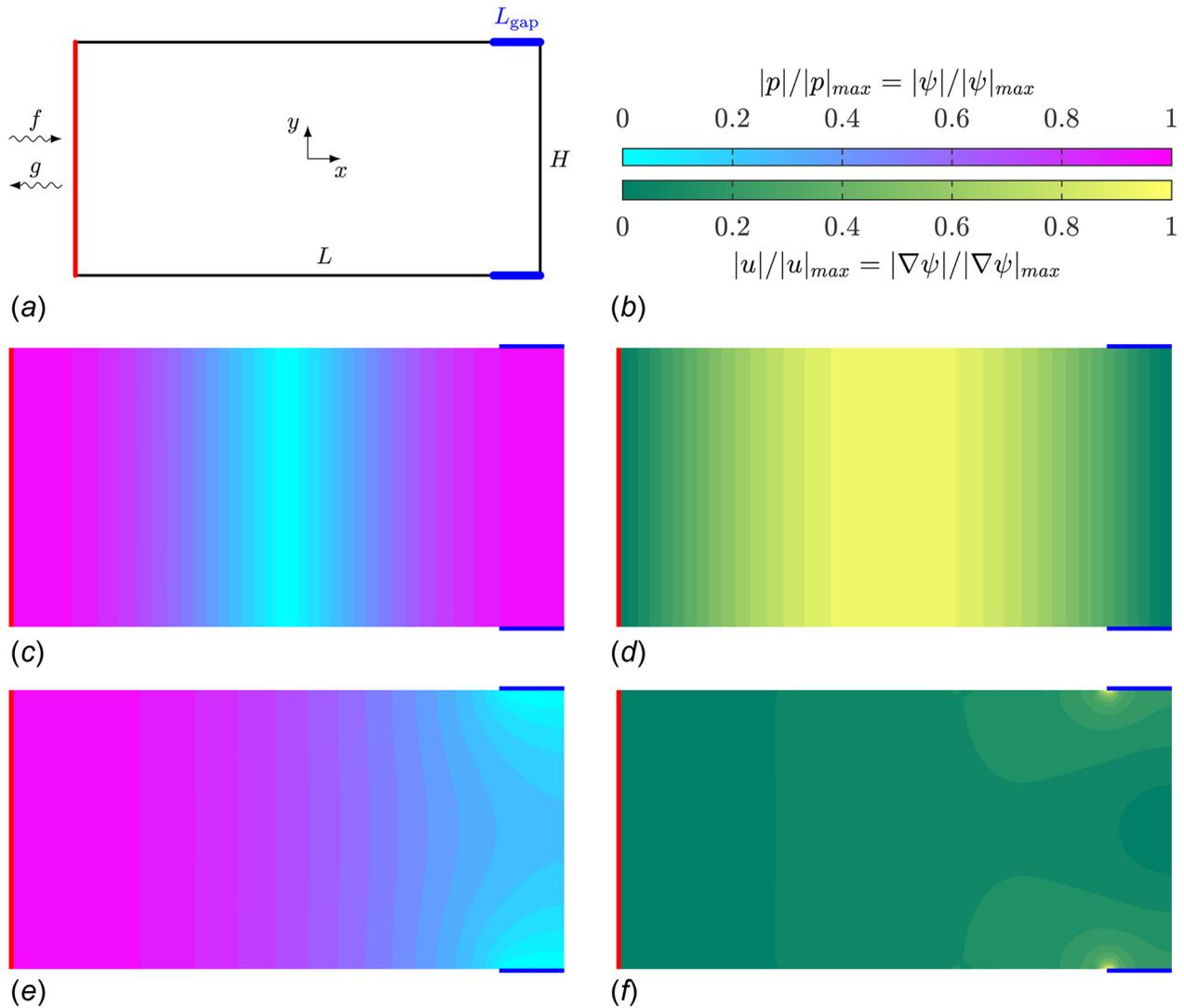
Fig. 2 (*a*) Geometry of the 2D model of the transition duct, simplified from the original geometry of Fig. 1. (*b*) Legend, common to the other four figures. ((*c*) and (*d*)) First nontrivial eigenmode of the studied geometry for an axial mode, i.e., $m = 0$ ($\lambda = 2L$). Absolute value of the acoustic pressure on the left and absolute value of the acoustic velocity on the right. The solutions of the axial case match the solutions of the problem with Neumann conditions applied over the whole boundary. ((*e*) and (*f*)) same of (*c*) and (*d*) but for a push–pull mode, i.e., $m = N/2 = 7$, for a set of $N = 14$ cans ($\lambda = 4.26L$). In (*f*), the acoustic velocity has a strong increase where the gap starts and is inhomogeneous over the gap length.

Table 1 Typical proportions of the transition duct of Fig. 2(*a*)

Nondimensional number	Reference value
L_{gap}/H	0.2
L/H	2

case $m = 2$ apply also to the other degenerate modes $m = 1, 3, \ldots, 6$ that are then not discussed in the following.

We present in Figs. 2(*c*) and 2(*d*) the first nontrivial axial[4] mode, eigensolution of the problem for $m = 0$. We observe that the wavelength λ and the mode shape match the half-wavelength acoustic mode of the duct, which is the solution of the problem with homogeneous Neumann boundary conditions on the whole boundary, i.e., for $L_{gap} = 0$. We present in Figs. 2(*e*) and 2(*f*) the first push–pull mode. This mode has a pressure anti-node at the upstream end of the transition duct in Fig. 2(*e*) and a quite clear pressure node at the transition duct outlet on the right of the

domain, so that it resembles a quarter-wave mode of the whole 2D duct. However, the acoustic velocity of this mode, presented in Fig. 2(*f*), has a strong peak around the location where the gap between cans starts. The acoustic velocity profile is a decreasing function of the axial coordinate along the gap length, suggesting that low order models should account for this strong gradient and cannot assume that the component of the acoustic velocity normal to the gap is constant along the gap.

For the axial mode, one easily observes by substituting $m = 0$ into Eq. (1) that the solution is the same in all the cans, and in particular, the phase of the mode is the same in the whole combustor, so that all cans oscillate in phase. For a push–pull mode, we have already discussed after Eq. (3) how adjacent cans should be in opposition of phase.

After analyzing the axial ($m = 0$) and push–pull ($m = N/2$) modes, we now discuss the general azimuthal degenerate case $m = 1, \ldots, N/2 - 1$,[5] which is harder to interpret because it gives rise to complex-valued solutions. This is expected mathematically

---

[4]For the axial case only, there is also a trivial solution: a mode that is constant in the whole domain at 0 Hz.

[5]The respective negative cases $m = -N/2 + 1, \ldots, -1$ are identical because of the reflection symmetry.

$|p|/|p|_{max} = |\psi|/|\psi|_{max}$
0   0.1   0.2   0.3   0.4   0.5   0.6   0.7   0.8   0.9   1

$-\pi$ $-\pi/2$ 0 $\pi/2$ π
Phase Angle, $\arg(\psi)$

(b)

(c)
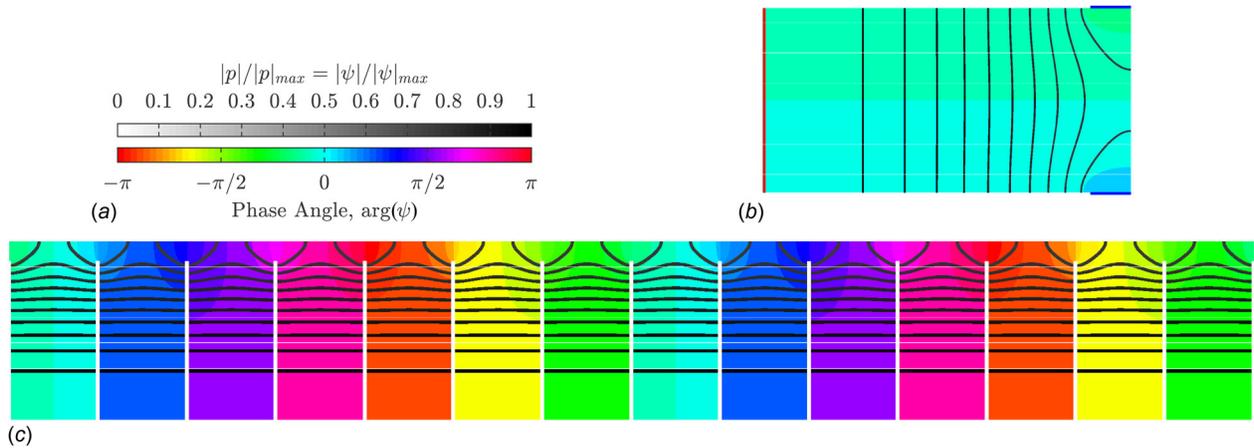
Fig. 3 First eigenmode with azimuthal order $m = 2$, for a set of $N = 14$ communicating cans. Because the solution is complex-valued, we use different colormaps for the absolute value and the phase angle, presented in the two legends in (a). In (b), we present the solution in one can only: we observe that the phase is approximately constant on the cross section at the upstream end of the transition duct, on the left, far from the cross-talk area. The amplitude decreases slightly from left to right. In (c), we present the ensemble of all the 14 cans pulsating together for the mode in (b), reconstructed using Eq. (1). The phase changes mostly at the cross-talk area and changes two times (since the azimuthal order m is 2) the quantity 2π along the annulus. At the upstream end of each transition duct, the phase is approximately constant and the mode presents a certain azimuthal phase pattern. The phase between two cans is the difference of the phase value between two locations. Refer to Fig. 4(a) for experimental evidence of a second-order azimuthal mode like this one in an engine. (a) Legend for (b) and (c). (b) First azimuthal $m = 2$ mode in one can, pressure field. Legend in (a). (c) Phase in the 14 cans of the same mode of (a). The first can from the left is the same appearing in (b).
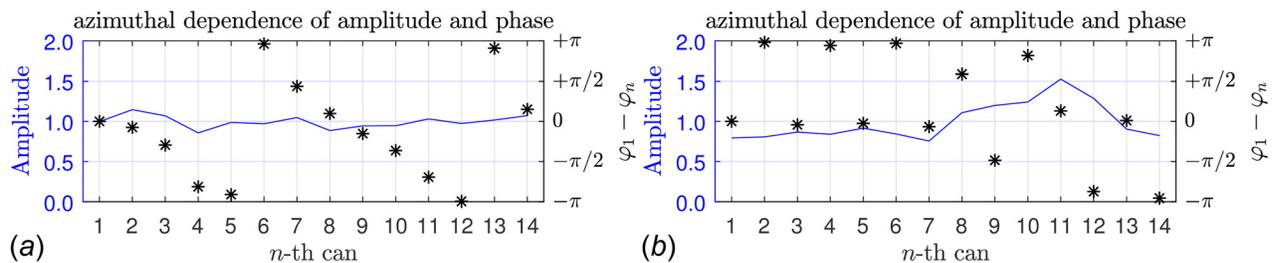
Fig. 4 Experimental evidence of a second azimuthal and of a push–pull mode. The timeseries of 14 pressure sensors in a 14-can can-annular combustor are processed at the frequency of one thermoacoustic instability. We present the amplitude of pulsation at that frequency on the left axis (in arbitrary units) and the phase difference on the right vertical axis at this frequency in each can. The phase difference is between the first can and the nth can, so that the value is zero in the first can. (a) and (b) refer to a different frequency of oscillation and a different operating condition. (a) The phase pattern corresponds to an azimuthal mode of order $m = 2$ that is rotating, because the phase changes with an approximately constant slope twice the amount of 2π moving along the annulus. This matches the theoretical prediction of Fig. 3(c). (b) The phase difference between most adjacent cans is very close to $\pm\pi$ ($m = N/2 = 7$). We observe some variation of the amplitude between cans, characterized as mode localization in The Effect of Asymmetry section of the paper.

because the term on the right-hand side of the boundary condition (4) is complex-valued, and physically because a spinning mode rotates in the annulus just before the turbine inlet with a varying phase in the azimuthal direction, and such phase is the argument of the eigenmode. We plot the first eigenmode for $m = 2$ in Fig. 3(b), where the colored filling represents the phase and the gray lines represent the absolute value. By exploiting Eq. (1) for $m = 2$, we reconstruct from the solution of a single can of Fig. 3(b) the solution in all the $N = 14$ cans, presented in Fig. 3(c). The phase is approximately constant within each can and describes how all the cans oscillate with the synchronization/phase pattern described by the azimuthal order m.

We conclude this paragraph by presenting in Fig. 4 evidence of a second-order azimuthal mode and of a push–pull mode based on engine data. Following the same methodology of Ref. [26], we present in Fig. 4(a) the phase pattern between pressure sensors located at different azimuthal locations, i.e., different cans. The pattern matches the predicted phase pattern presented in Fig. 3(c)

for a second azimuthal mode. Figure 4(b) presents a pulsation pattern where adjacent cans oscillate out of phase, compatible with a push–pull mode. Similar experimental evidence based on two cans only is presented by Farisco et al. [12] in their Fig. 1. However, in Fig. 4(b), some adjacent cans are not exactly out of phase, and we observe some variation of the amplitude of the mode as a function of the can number. We will reconsider these two features later.

Equivalent Reflection Coefficient. We now turn our attention to the reflection coefficient $R = g/f$ observed from the inlet of the transition duct, sketched with the red line in Fig. 2(a). In particular, we discuss how a certain mode, either axial, azimuthal, or push–pull, traveling downstream in one can with amplitude f, is reflected back with amplitude g from the ensemble of the other transition ducts. This can be calculated with a Green function approach on the problem by expanding the Green function as a truncated Galerkin series [27, §7.3]. This is a consolidated
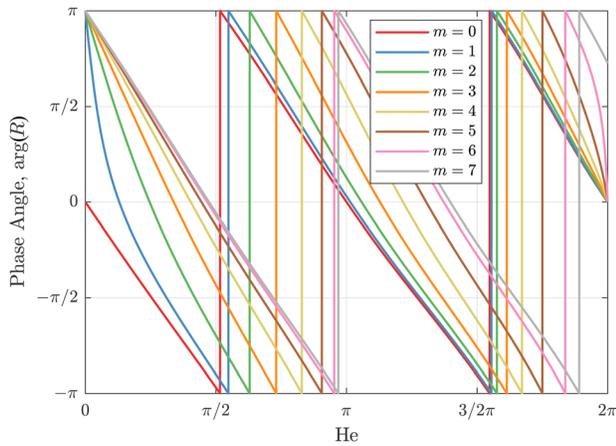
Fig. 5   Phase of the equivalent reflection coefficient for the azimuthal modes for $N = 14$ cans, calculated with reference cross section at the red inlet of the transition duct of Fig. 2(a). The Helmholtz number is defined as He $= L\omega/c$.
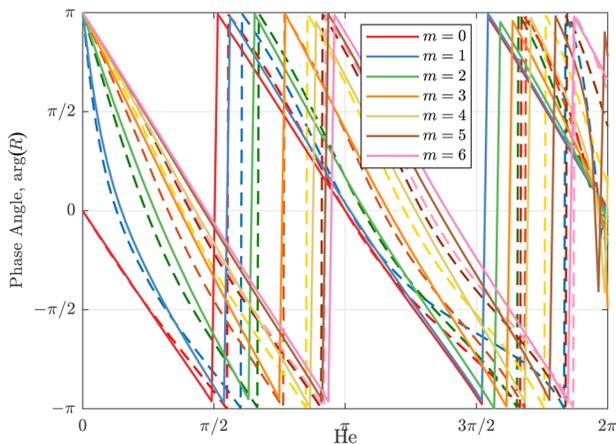
Fig. 6   Validation of the geometrical simplifications for the 2D model for $N = 12$. The dashed lines are obtained from a fixed complex 3D geometry, while the continuous lines are obtained with the bidimensional model proposed in this paper, with the nondimensional values estimated from the 3D geometry without applying further corrections. The good agreement validates the geometrical approximations made to map the complex 3D geometry to the simpler 2D model.

technique that requires the calculation of all the eigenmodes in the frequency range of interest [28]. One obtains the impedance $\tilde{Z}_m$

$$p_m = \tilde{Z}_m u_m \tag{5}$$

$\tilde{Z}_m$ relates the pressure and the acoustic velocity at the inlet of one transition duct, assuming all other ducts respond at the azimuthal wavenumber m. The gain of the reflection coefficient $R_m = (Z_m - 1)/(Z_m + 1)$ is trivially one at all frequencies because we do not consider any acoustic losses. The phase of R for different modes is presented in Fig. 5, for the nondimensional values fixed in Table 1. We present the results as a function of the Helmholtz number He, defined as

$$\text{He} = \frac{L\omega}{c} \tag{6}$$

When interpreting the results, it is useful to observe that He $= \pi$ corresponds to the frequency of the first nontrivial axial mode[6] of Fig. 2(c).

---

[6]Because that mode has a wavelength $\lambda = 2L$, see Fig. 2(c).
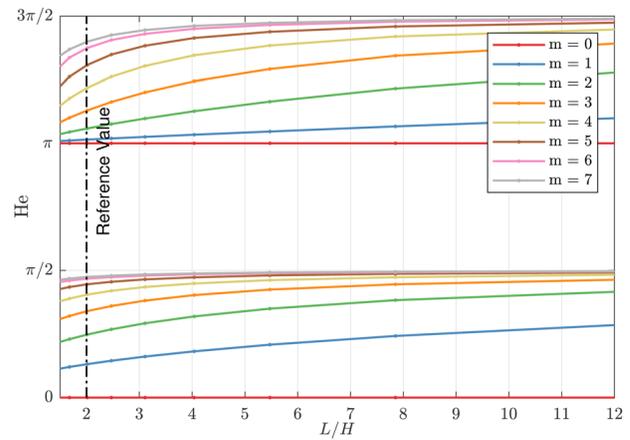
Fig. 7   Sensitivity of the first two eigenfrequencies of a can system as a function of the geometry aspect ratio L/H, for all azimuthal wavenumber m, for $N = 14$. We plot the Helmholtz number of all the eigenmodes with He $< 2\pi$ for each azimuthal mode m, as a function of the two nondimensional parameters governing can to can acoustic communication. As L/H increases, the Helmholtz number of the azimuthal modes converges slowly to $\pi/2$ and $3\pi/2$ for the first two modes. For a fixed value of L/H, the eigenfrequencies for $m = 5, 6, 7$ are rather close, forming a cluster. These modes are closer together the larger is L/H.

We observe that in the zero frequency limit, the ensemble of transition ducts behaves like a wall for the axial mode ($R = 1$), while it behaves as an open end for all azimuthal modes ($R = -1$). This is explained mathematically by the fact that the Galerkin series of the axial mode has a Helmholtz mode at $\omega = 0$, while all others do not. Modes with a high azimuthal wavenumber, e.g., $m \in \{5, 6, 7\}$, have a very similar phase response. In the linear regime, the solution is a superposition of these eigenmodes, which are linearly independent and orthogonal. This means that if there is an eigenmode at $m = 6$, very likely there exist also eigenmodes at $m = 5, 7$ with a very close frequency of oscillation. We call a set of modes with close frequencies a cluster, which we will further substantiate later.

We present in Fig. 6 a comparison between the results obtained with a finite element solver on a complex 3D geometry of 12 connected transition ducts neglecting mean flow and results obtained with the 2D model presented in this paper. The good agreement confirms that the ignored geometrical features play a minor role and further validates the 2D model.

Eigenfrequencies. In Fig. 7, we study the sensitivity of the eigenfrequencies of the system with respect to the aspect ratio L/H. We study the Helmholtz number He $= \omega L/c$ of the eigenmodes, with the number defined so that the half-wave mode presented in Figs. 2(c) and 2(d) has a Helmholtz number equal to π. We observe that as the aspect ratio L/H increases, the frequencies of the azimuthal modes slowly get closer to the frequency of the push–pull mode, to one of the two horizontal asymptotes at He $= \pi/2$ and He $= 3\pi/2$.

One can also make use of Fig. 7 to discuss the eigenfrequencies of a whole can-annular combustor. In fact, a combustor where all cans do not communicate on the upstream end at the plenum, or such that this communication at the plenum plays a negligible role, can be modeled with a set of noncommunicating cylinders connected on the upstream end to the transition ducts. This is simply an increase of the length L of the computation domain of Fig. 2(a). For example, the eigenfrequencies of a can combustor with a can equivalent[7] total length that is thrice the transition duct

---

[7]The upstream part of the can is often colder, so that the equivalent length at the temperature of the transition duct is longer than the actual geometrical length.
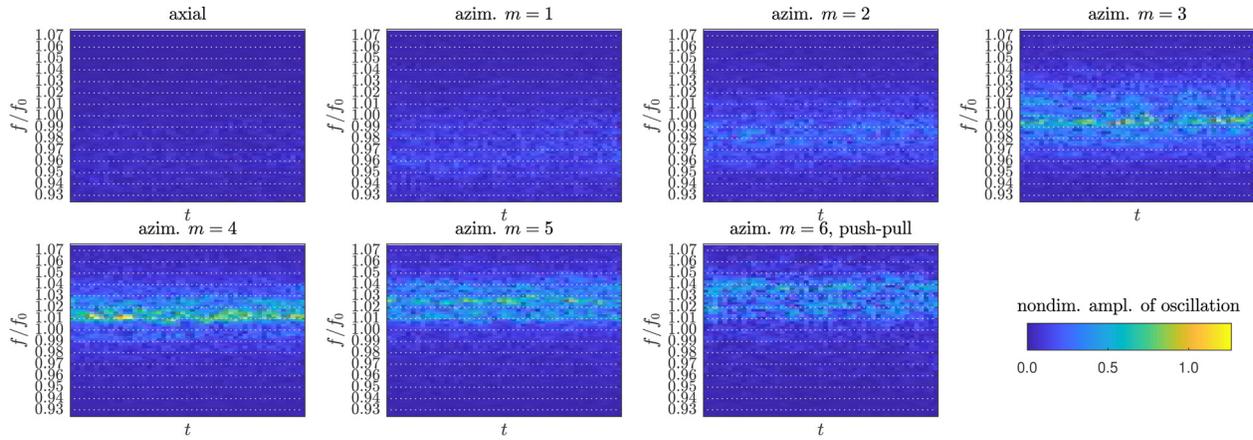
Fig. 8 Spectrogram of the timeseries of the azimuthal modes reconstructed from an engine. We can observe that more than one azimuthal mode is active in a small range of frequencies, forming a cluster. Within the cluster, each mode peaks at a frequency that increases with the azim. order _m_. The highest amplitude is not always in the same mode, and the system's energy appears to move randomly between the modes, with some statistical preference for the _m_ = 3, 4, 5 modes.

length can be read in Fig. 7 by setting the aspect ratio L/H to 6. We observe that the eigenfrequencies of the high azimuthal wavenumbers $m \in \{5, 6, 7\}$ are all very close and form a cluster. One can then expect that this cluster may occur together in experimental measurements, if one considers the system in a linear framework, and subject to stochastic noise and weak nonlinear saturation.

To experimentally validate this, from the pressure value $p^{(n)}$ at a fixed axial location in the nth can, upstream of the transition duct, we introduce the amplitude p_m of the mth azimuthal mode with the discrete Fourier transform

$$p_m = \frac{1}{N} \sum_{n=1}^{N} p^{(n)} e^{-im\theta_n} \qquad (7)$$

In Eq. (7), $m = -N/2 + 1, \ldots, 0, 1, \ldots, N/2$ is the azimuthal wavenumber, and the angle θ_n is defined in Eq. (2). We present in Fig. 8 the spectrogram of the azimuthal modes of an engine. One then observes the experimental evidence of the clusters just predicted, where the system selects certain azimuthal modes in which it expresses larger acoustic amplitudes based on factors like the flame response at the different modes' frequencies, and the loss of rotational symmetry of the system, as discussed in The Effect of Asymmetry section.

Based on this evidence on thermoacoustic clusters, we look again at the phase pattern for the push–pull mode presented in Fig. 4(_b_). Because close to the push–pull mode frequency, there are other modes of high azimuthal order that may also be excited, the phase pattern of Fig. 4(_b_) for $m = 7$ is not as clean as if only one mode is excited, as in Fig. 4(_a_). The nonuniform amplitude pattern will be discussed later.

Transmission Between Cans. In the Eigenfrequencies section, we have calculated the response of the set of N transition ducts to the mth azimuthal mode. This has allowed to understand experimental data, both in terms of frequencies and phase pattern, on a system level. With the same information, one can also discuss the acoustic response in terms of individual cans. In particular, one considers the ensemble of N communicating transition ducts, with N ports at the outlet of the N cans, i.e., at the inlet of the transition ducts. The communication between these N ports can be written as a many-to-many impedance between the pressures $\boldsymbol{p} \equiv [p^{(1)}, \ldots, p^{(N)}]$ and the velocities $\boldsymbol{u} \equiv [u^{(1)}, \ldots, u^{(N)}]$ at the inlet of each transition duct

$$\frac{p^{(n)}}{\rho c} = \sum_{m=-N/2+1}^{N/2} \frac{p_m}{\rho c} e^{im\theta_n} = \sum_{m=-N/2+1}^{N/2} \tilde{Z}_m u_m e^{im\theta_n} \qquad (8)$$

where Eq. (5) has been substituted in the second passage in Eq. (8). In Eq. (8), ρ is the mean density of the gas and we use superscript within round parentheses to refer to quantities calculated in can space. One then writes the acoustic velocities of the azimuthal modes u_m in terms of the velocities in the cans

$$\frac{p^{(n)}}{\rho c} = \sum_{m=-N/2+1}^{N/2} \tilde{Z}_m \left(\frac{1}{N} \sum_{q=1}^{N} u^{(q)} e^{-im\theta_q} \right) e^{im\theta_n} \qquad (9)$$

$$= \sum_{q=1}^{N} \underbrace{\left(\frac{1}{N} \sum_{m=-N/2+1}^{N/2} \tilde{Z}_m e^{im(\theta_n - \theta_q)} \right)}_{Z^{(nq)}} u^{(q)} = \sum_{q=1}^{N} Z^{(nq)} u^{(q)} \qquad (10)$$

Instead of characterizing the response in terms of $p^{(n)}$ and $u^{(n)}$, we can look at the problem in terms of the Riemann invariants $f^{(n)}$ and $g^{(n)}$ axial in each can, with f and g as sketched in Fig. 2(_a_). They are related as $\boldsymbol{g}(\omega) = \boldsymbol{T}(\omega) \boldsymbol{f}(\omega)$, where $T^{(nq)}$ are calculated from $Z^{(nq)}$. The operator $T^{(nq)}$ expresses the transmission of the downstream traveling wave $f^{(q)}$ leaving the qth can and being converted into an upstream traveling wave $g^{(n)}$ entering the nth can. For $n = q$, we have that $T^{(nn)}$ expresses the reflection of $f^{(n)}$ back upstream to the same can. Both $\boldsymbol{Z}(\omega)$ and $\boldsymbol{T}(\omega)$ are circulant matrices at a fixed frequency ω and hold a series of elegant mathematical properties [29]. Physically, this happens because of the rotational symmetry of the system, so that for example $T^{(3,8)}(\omega)$ is identical to $T^{(4,9)}(\omega)$ because the system is invariant to a rotation of the azimuthal frame of reference of one can. It follows that the transmission matrix $\boldsymbol{T}(\omega)$ is fully defined by a single row or column, so we introduce

$$T^{(d)} = T^{(1,d+1)} \quad d = 0, 1, \ldots, N/2 \qquad (11)$$

which is the transmission of a wave f traveling downstream one can to a can that is d cans apart. In particular for $d = 0$, we have that $T^{(0)} f$ is the reflected wave in the same can, $T^{(1)} f$ the transmitted wave in each of the two adjacent cans, and so on as sketched in Fig. 9(_a_). Because of the mirror symmetry, we also have that
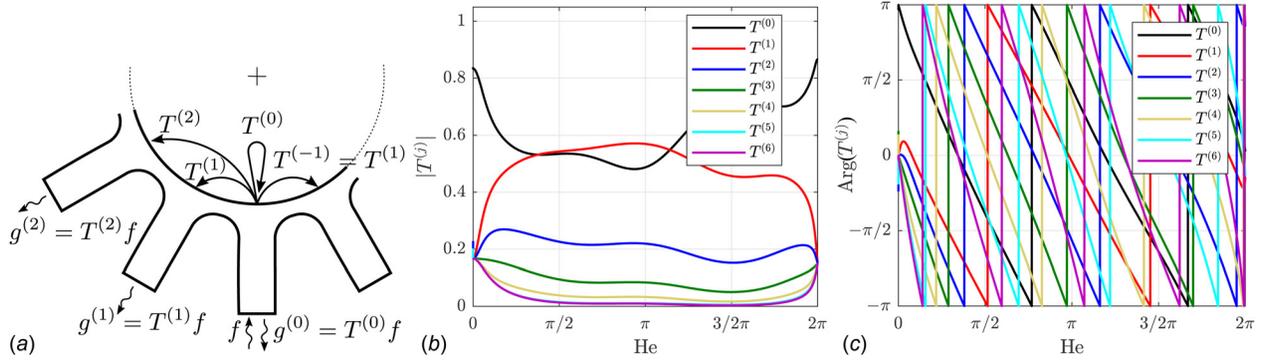
Fig. 9 (*a*) Sketch of the reflection/transmission transfer functions $T^{(d)}$ for an incoming traveling wave *f*. Each function $T^{(d)}(\omega)$ is the transmitted Riemann invariant from one can to a can that is *d* cans apart. For example, $T^{(0)}$ is the reflection of a wave propagating downstream of one can and being reflected to the same can, and $T^{(3)}$ can be interpreted for example as the transmission of a wave traveling downstream can 4 and propagating upstream in can 7, or any other two cans that are 3 cans apart. ((*b*) and (*c*)) Gain and phase of the transfer functions $T^{(d)}$ between all cans.

$T^{(k)} = T^{(N-k)}$, so that only $N/2 + 1$ elements of $T^{(d)}$ need to be defined. It is then sufficient to characterize the transfer functions from one can to itself and to the first $N/2$ cans in either clockwise or anti-clockwise direction to fully describe T.

We present in Figs. 9(*b*) and 9(*c*) the transfer functions $T^{(d)}$ for $d = 0, 1, \ldots, N/2$. We observe how the transmission is stronger to cans that are close to the originating can. Moreover, in the zero Helmholtz number limit, the gain of $T^{(0)}$ goes to $1 - 2/N$, while the gain of all other $T^{(j)}$ $j \neq 0$ goes to $2/N$.

We observe that the reflection of a wave to the same can has a phase response of π at the origin, i.e., the turbine inlet behaves as an open duct if all other cans do not respond. This is not the case in practice, and one should not draw conclusions on the system's dynamics based on the results of Fig. 9, because the synchronization and interaction between the cans is not accounted for. One can instead discuss the reflection of a wave back to the same can for all possible synchronized states of the other pulsating cans, as presented already in Fig. 5. One can then argue that the nonlinear, stochastic response of all other cans will lie somewhere inbetween all the responses of these possible synchronized states in a statistical sense.

The Effect of Asymmetry

In this section, we will introduce and study a simplified can-annular system in terms of a network model. Based on this model system, we will perform a modal analysis without and with flame response to illustrate the general eigenstructure of this type of system. We will furthermore assess the effect of asymmetry, originating from different flame responses in the cans, as this may occur in an engine, on purpose or not.

Modal and stability analyses including the effect of asymmetry have been conducted for annular combustors in various studies (for example, see Refs. [2,15,30]); however, it can be expected that a can-annular system exhibits qualitatively different eigenstructures and response to asymmetries. This is because a can-annular system can be interpreted as a system of weakly coupled, nominally identical oscillators, from which it inherits certain dynamical features. For an annular system, this interpretation is not appropriate. The aspect that applies to both annular and can-annular systems is the discrete rotational symmetry, at least nominally. Since both types of systems feature the same symmetry group, eigenvalue degeneracy, and associated splits under asymmetric perturbations are identical. However, as pointed out in the Rotationally Symmetric Case section and is further elaborated on below, the eigenfrequencies for can-annular systems come in clusters (associated with a certain axial mode order in the cans), which is a result of the weak coupling and cannot be found in annular systems. As is well known in general modal theory [31], systems with eigenvalue clusters (i.e., eigenvalues that are close) feature

high eigenfunction sensitivity toward perturbations. Therefore, a can-annular system that is only slightly asymmetrically perturbed may exhibit significant changes in the oscillation pattern, vastly different from the mode structures in the symmetric case. We will illustrate these effects on the basis of a model system introduced next. To account for the can-to-can coupling in a realistic fashion, we use the impedance/reflection coefficient matrix of the transition duct arrangement discussed in the Rotationally Symmetric Case section.

The cans are modeled in a simplified manner through, starting from the upstream end, as sketched in Fig. 10:

(1) a pressure-node impedance, representing the large volume of the plenum, imposing a pressure-release condition;
(2) an $L - \zeta$ model [32], representing the burner;
(3) a flame transfer function;
(4) a duct, accounting for the acoustic propagation from the flame to the transition duct.

For the $L - \zeta$ model, we choose an effective length of 10% of the transition duct length, which is a realistic value for swirl generators; the damping coefficient ζ is set to zero here, as we do not attempt any quantitative comparison with experimental data. The can length is set equal to the transition duct length, for a total length of $2L$. The ratio of burned to unburned gas temperature is set to 2.5, representative of the ratio of lean flame temperature to compressor outlet temperature. The changes in molar mass and ratio of specific heats from unburned to burned state are neglected. We consider a can-annular system with 12 cans.

On the upstream side, the can models are uncoupled. This is evidently a simplification, as there is acoustic communication through the plenum. However, since the burner pressure loss is
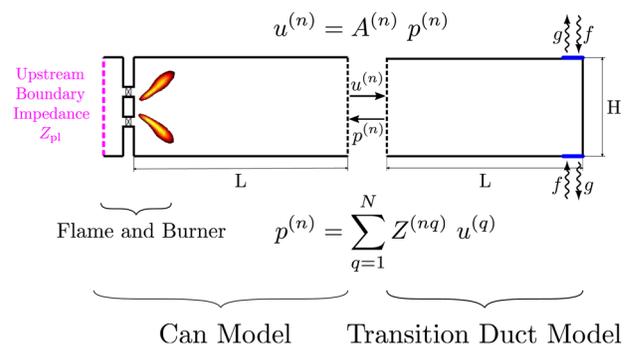
Fig. 10 Sketch of the *n*th can of the can-annular model. The can communicates with the others via the blue cross-talk area where the *f*, *g* waves are sketched.

typically significant, we expect that the dominant acoustic communication occurs through the gap in the transition duct at the turbine inlet. We also neglect pairwise can-to-can communication through cross-fire tubes, as these have typically small cross-sectional areas.

The eigenfrequencies and corresponding azimuthal modal pressure distributions are obtained as follows. We use the impedance matrix in can space, $\mathbf{Z}(\omega)$, as introduced in Eq. (10), whose nqth element maps the acoustic velocity at the upstream end of the transition duct in can q to the acoustic pressure in can n at the same axial location. Furthermore, we combine transfer matrices and boundary condition of the elements upstream of the transition duct, i.e., duct, flame response, burner, and upstream impedance, into a scalar admittance for each can, $A^{(n)}(\omega)$, with can index n

$$A^{(n)} = \frac{-\mathrm{i}\xi \tan(k_h L)\big(Z_{\mathrm{pl}} - \zeta M - \mathrm{i}k_c L_b\big) + 1 + (T_h/T_c - 1)\mathcal{F}_n(\omega)}{\xi\big(Z_{\mathrm{pl}} - \zeta M - \mathrm{i}k_c L_b\big) - \mathrm{i}\tan(k_h L)\big(1 + (T_h/T_c - 1)\mathcal{F}_n(\omega)\big)}$$

Here, Z_{pl} is the plenum impedance (set to zero), k_c and k_h are wavenumber upstream and downstream of the flame, respectively, ξ is the ratio of characteristic impedances on the hot and cold side, M is the burner Mach number, L_b the effective length of the burner, T_h and T_c temperatures on the burned and unburned side, respectively, and $\mathcal{F}_n(\omega)$ the flame transfer function in the nth can. Instead of choosing one of the many flame transfer function models available in the literature, we choose a form that is most appropriate for our purpose

$$\mathcal{F}^{(n)} = g^{(n)}e^{-\mathrm{i}\pi/2} \tag{12}$$

where we will assign different values to the gain g_n in the following. By fixing a constant phase to $\mathcal{F}^{(n)}$ in Eq. (12), all modes in one cluster of eigenfrequencies will be very similarly amplified. This is because when the eigenfrequencies are close, the axial mode shape is similar, and this leads to similar Rayleigh driving. Moreover, if we consider the first cluster of eigenfrequencies, which is associated with an axial quarter-wave mode that has a node at the upstream end, a phase of $-\pi/2$ provides maximum driving for the purely acoustic modes. (Note that this does not necessarily hold for the thermoacoustic modes for which the maximum driving may be attained for a slightly different phase.)

The upstream can admittance can be written as a frequency-dependent scalar function because the cans are assumed uncoupled on the upstream side. In order to formulate the dispersion relation for the system in a compact fashion, we introduce the upstream impedance matrix $\mathbf{A}(\omega)$, which is diagonal and has elements $(\mathbf{A})^{(nq)} = A^{(n)}\delta_{nq}$. Analogous to the can impedance matrix $\mathbf{Z}(\omega)$, the element nq of the admittance matrix maps the pressure in can q to the acoustic velocity in can n, upstream of the transition duct. If all cans are identical upstream of the transition duct, the admittance matrix $\mathbf{A}(\omega)$ is a multiple of the identity matrix and then also circulant. However, if we allow for different flame responses among the cans, $\mathbf{A}$ is still diagonal but the diagonal entries will generally be different so that $\mathbf{A}$ is no longer circulant. Now for the pressure field to be continuous at the upstream end of the transition duct, we require

$$\mathbf{Z}(\omega)\mathbf{A}(\omega)\boldsymbol{p} = \boldsymbol{p}$$

which induces the dispersion relation

$$\det[\mathbf{Z}(\omega)\mathbf{A}(\omega) - \mathbf{I}] = 0 \tag{13}$$

where $\mathbf{I}$ is the $N \times N$ identity matrix. Solutions ω_k to Eq. (13) are the system's eigenvalues, $\mathrm{Re}(\omega_k)$ and $\sigma_k \equiv -\mathrm{Im}(\omega_k)$ corresponding to angular oscillation frequency and growth rate of the kth mode, respectively. The associated modal pressure distribution (the eigenvector $\boldsymbol{p}_k$) is then obtained as the nullspace of the system matrix evaluated at the eigenfrequency [30]
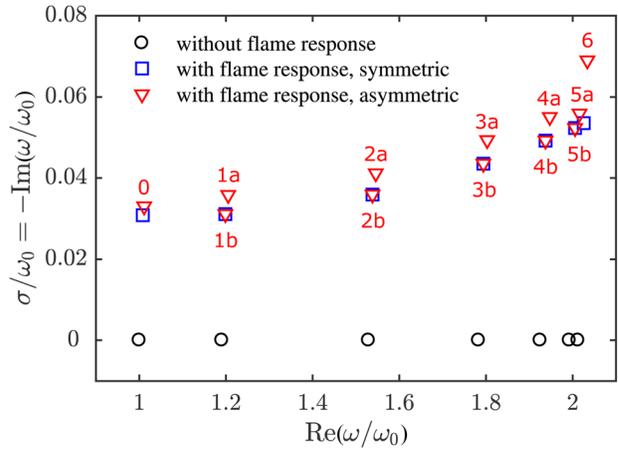
Fig. 11 Complex eigenvalues for the three cases considered. The eigenvalues have been normalized with the angular eigenfrequency of the quarter-wave mode of an isolated can. The vertical axis is the normalized growth rate of oscillation of each mode. The red numbers refer to the asymmetric case and describe the mth azimuthal order of the respective symmetric eigenmode. The amplitude and phase of each asymmetric mode is presented in Fig. 12 in the plot with the same red number in the top left corner.

$$\boldsymbol{p}_k = \ker[\mathbf{Z}(\omega_k)\mathbf{A}(\omega_k) - \mathbf{I}]$$

The dimension of the kernel corresponds to the geometric multiplicity and thus indicates whether the eigenvalue is degenerate.

We examine the system eigenvalues for three different cases: (i) there is a temperature increase across the flame but no flame response; (ii) the flame response is identical in all cans and set according to Eq. (12) with a gain $g^{(n)} = 0.2$; and (iii) the flame response is set as for case (ii), except for the first can, where the gain is increased to $g^{(1)} = 0.6$. The lowest cluster of eigenvalues, corresponding to an axial quarter-wave mode in the cans, are displayed for the three cases in Fig. 11. The eigenvalues have been normalized by the angular eigenfrequency of the quarter-wave mode in an isolated can, ω_0. We consider the case without flame response (black circles) first. As there is no damping included in the model, all eigenvalues are purely real (neither damped nor amplified). There are seven distinct eigenvalues in one cluster, two of which are simple; the other five have algebraic multiplicity two. The two simple eigenvalues correspond to azimuthal mode orders zero and six and the degenerate ones to azimuthal orders two to five. This can be predicted entirely based on the system's symmetry [30], but we will not repeat these arguments here for the sake of brevity. The eigenvalues with homogeneously distributed flame response (blue squares) all have negative imaginary part (positive growth rate) and are thus unstable. Furthermore, no splitting of degenerate eigenvalues is observed, as the flame response preserves the full symmetry.

For case (iii), in which the gain of the flame response in the first can is increased by a factor of three (red triangles), part of the eigenvalues exhibit larger growth rates. Furthermore, all initially degenerate modes are split because the system does not feature any discrete rotational symmetry anymore. This is consistent with arguments based on the system's symmetry group [30] or the so-called C_{2n} criterion [32]. One of the two split modes associated with an initially degenerate eigenvalue is seen to remain unaltered with respect to the symmetric case. This is because the pressure distributions corresponding to azimuthal orders one to five can be oriented such that they have a node in the first can so that the increased flame response gain has no effect. One striking feature is that the mode with the highest oscillation frequency also exhibits its a distinctly larger growth rate.
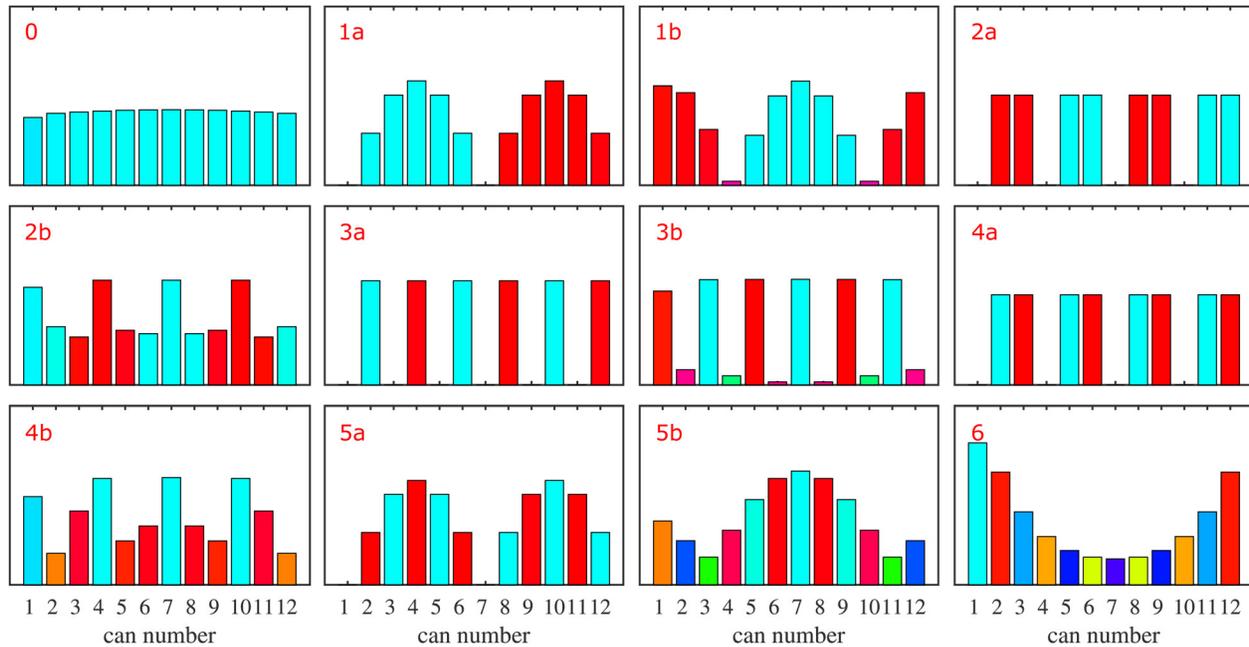
Fig. 12 Visualization of the azimuthal mode shapes associated with the eigenvalues of the asymmetric case (Fig. 11). Ordered from left to right and top to bottom with increasing oscillation frequency. The bar height indicates the pressure amplitude and the bar color the phase (same color legend as in Fig. 3), at the interface between each can and each transition duct. The number in the top left corner is the azimuthal order _m_ of the corresponding mode in the symmetric case. Couple of modes with the same _m_ differ very little in frequency and can result in a slowly modulated linear combination with approximately constant amplitude along the annulus. This is not the case for the perturbed push–pull mode in the bottom right corner, where cans 1, 2, 3, 10, 11, and 12 present much larger amplitude than the others.

We consider the mode shapes in the form of azimuthal pressure distribution at the inlet of the transition ducts next (Fig. 12). Only those corresponding to the asymmetric case are shown. For the symmetric cases, the system matrix $\mathbf{ZA} - \mathbf{I}$ is circulant, and all eigenvectors are discrete Fourier modes, as presented earlier in this paper and in Ref. [29]. While the modes corresponding to the lower eigenfrequencies are almost unaffected by the asymmetry, those with higher azimuthal order are seen to strongly differ from the symmetric case. The mode with the highest oscillation frequency (bottom right) is affected most; this is also the mode that gains the biggest increase in growth rate through the asymmetry (Fig. 11). In fact, this mode shape is quite different from all the modes corresponding to the symmetric case (the discrete Fourier modes) and presents an increased amplitude level in a set of neighboring cans. We discuss next experimental evidence of this pattern.

Goldmeer et al. [33, Fig. 14] show a pulsation pattern for a GE gas turbine that strongly resembles the amplitude pattern of Fig. 12, bottom right frame ($m = 6$). Also, the experimental results of Fig. 4(*b*) show a larger amplitude in the subset of cans 8–12 that can be caused by a locally increased flame response due to loss of perfect symmetry of the system. We observe that this mode localization can be caused by other local perturbation of the symmetry, i.e., a change in the geometry in one can can lead to a similar perturbation of the problem and resulting pulsation pattern. This explains the experience of Calpine on how increased pulsation levels in certain cans can be related to localized hardware damage. In particular, Sewell and Sobieski [34, Fig. 7.13] present experimental evidence that a transition piece mechanical failure is linked to the onset of thermoacoustic oscillations localized in the same can and few neighboring cans.

A relatively small asymmetric perturbation can, thus, have a drastic impact on the azimuthal pressure distribution in a can-annular system. This effect is indeed reminiscent of mode localization, a phenomenon that is frequently observed in slightly asymmetric, weakly coupled systems [35].

Conclusions

In this paper, we introduce a low-order model for the acoustic communication at the turbine inlet between the transition ducts of can-annular combustors with _N_ cans. We use the model to discuss the mode shapes and eigenfrequencies of can-annular combustors. We predict how azimuthal modes correspond to certain synchronization patterns of the phases between the axial acoustic pressure in the cans. We validate these patterns with engine data of a 14-can combustor.

We discuss the equivalent reflection coefficient of the set of _N_ transition ducts for a thermoacoustic mode of a certain azimuthal order _m_. We present the asymptotic behavior in the zero Hz limit and its physical interpretation. We study the eigenfrequencies of can-annular systems as a function of the overall axial length of the cans and predict the occurrence of clusters of eigenmodes with very close frequencies. Within a cluster, the frequencies of the modes are increasing as a function of the azimuthal order _m_ of the modes. These clusters are a peculiar feature of can-annular combustors as opposed to annular combustors. We present experimental evidence of these clusters with engine data of a 12-can combustor.

After analyzing the problem from a system perspective in the space of the azimuthal modes, we change perspective and discuss the direct interaction between each pair of the _N_ cans. We show how the two perspectives are linked by the discrete Fourier transform in the spatial azimuthal direction. We discuss how at low frequencies the coupling strength between two cans depends on their distance. As a result, in this low frequency regime, an axial acoustic wave traveling downstream a fixed transition duct is primarily reflected back, and only partially transmitted to the other cans. Of the transmitted part, the strongest transmission occurs toward the two closest neighboring cans. This suggests that the coupling between cans is low, as compared to the feedback loop of each can with itself due to the reflection, and that we can look at the set of _N_ cans as a set of weakly coupled oscillators. Because the strength of the coupling is stronger between cans that are

close, synchronization between neighboring cans is stronger when a whole cluster of modes is excited in the system.

We finally discuss the effect of a loss of rotational symmetry in the system and show that it is responsible of mode localization. We start with a model of a symmetric can-annular combustor with $N = 12$ cans and artificially increase the response of the flame in can number 1, to mimic a generic local change of the system. We find that the shapes of the eigenmodes forming the cluster present a strong sensitivity against this perturbation. This strong sensitivity is typical of systems that show clusters of eigenmodes and is then a peculiar feature of can-annular combustors, as opposed to annular combustors, which do not exhibit clusters nor a strong sensitivity of the mode shapes on the loss of rotational symmetry. We observe that in the can with a stronger flame response, the push–pull mode shows the strongest change both (1) in the amplitude pattern, with a strong increase of amplitude in the same can, and to a smaller extent to its neighbors; (2) in the growth rate, in particular in a linear framework it is the mode by far excited the most. We then review how the pulsation amplitude pattern of this mode has been experimentally observed in three different engines. In one case, this was found to be caused by a localized structural damage in one can.

References

[1] Pennell, D. A., Bothien, M. R., Ciani, A., Granet, V., Singla, G., Thorpe, S., Wickstroem, A., Oumejjoud, K., and Yaquinto, M., 2017, "An Introduction to the Ansaldo GT36 Constant Pressure Sequential Combustor," ASME Paper No. GT2017-64790.

[2] Noiray, N., Bothien, M., and Schuermans, B., 2011, "Investigation of Azimuthal Staging Concepts in Annular Gas Turbines," Combust. Theory Modell., 15(5), pp. 585–606.

[3] Connor, J. O., Acharya, V., and Lieuwen, T., 2015, "Transverse Combustion Instabilities: Acoustic, Fluid Mechanic, and Flame Processes," Prog. Energy Combust. Sci., 49, pp. 1–39.

[4] Bothien, M., Noiray, N., and Schuermans, B., 2015, "Analysis of Azimuthal Thermo-Acoustic Modes in Annular Gas Turbine Combustion Chambers," ASME J. Eng. Gas Turbines Power, 137(6), p. 061505.

[5] Bauerheim, M., Nicoud, F., and Poinsot, T., 2016, "Progress in Analytical Methods to Predict and Control Azimuthal Combustion Instability Modes in Annular Chambers," Phys. Fluids, 28(2), p. 021303.

[6] Krebs, W., Bethke, S., Lepers, J., Flohr, P., Prade, B., Johnson, C., and Sattinger, S., 2005, "Thermoacoustic Design Tools and Passive Control: Siemens Power Generation Approaches," Combustion Instabilities in Gas Turbine Engines: Operational Experience, Fundamental Mechanisms, and Modeling (Progress in Astronautics and Aeronautics), T. Lieuwen and V. Yang, eds., American Institute of Aeronautics and Astronautics, Arlington, TX, pp. 89–112.

[7] Macquisten, M. A., Whiteman, M., and Moran, A. J., 2004, "Application of Low Order Thermo-Acoustic Network to DLE Staged Combustor," ASME Paper No. GT2004-54161.

[8] Kaufmann, P., Krebs, W., Valdes, R., and Wever, U., 2008, "3D Thermoacoustic Properties of Single Can and Multi Can Combustor Configurations," ASME Paper No. GT2008-50755.

[9] Farisco, F., Panek, L., Janus, B., and Kok, J. B. W., 2015, "Numerical Investigation of the Thermo-Acoustic Influence of the Turbine on the Combustor," ASME Paper No. GT2015-42071.

[10] Farisco, F., Panek, L., and Kok, J. B. W., 2016, "Thermo-Acoustic Cross-Talk Between Cans in a Can-Annular Combustor," International Symposium on Thermoacoustic Instabilities in Gas Turbines and Rocket Engines, Munich, Germany, May 30–June 2, pp. 1–12.

[11] Panek, L., Huth, M., and Farisco, F., 2017, "Thermo-Acoustic Characterization of Can-Can Interaction of a Can-Annular Combustion System Based on Unsteady CFD LES Simulation," First Global Power and Propulsion Forum, Zurich, Switzerland, Jan. 16–18, Paper No. GPPF-2017-81.

[12] Farisco, F., Panek, L., and Kok, J. B., 2017, "Thermo-Acoustic Cross-Talk Between Cans in a Can-Annular Combustor," Int. J. Spray Combust. Dyn., 9(4), pp. 452–469.

[13] Stow, S. R., and Dowling, A. P., 2003, "Modelling of Circumferential Modal Coupling Due to Helmholtz Resonators," ASME Paper No. GT2003-38168.

[14] Mensah, G. A., and Moeck, J. P., 2016, "Efficient Computation of Thermoacoustic Modes in Annular Combustion Chambers Based on Bloch-Wave Theory," ASME J. Eng. Gas Turbines Power, 138(8), p. 081502.

[15] Bauerheim, M., Cazalens, M., and Poinsot, T., 2015, "A Theoretical Study of Mean Azimuthal Flow and Asymmetry Effects on Thermo-Acoustic Modes in Annular Combustors," Proc. Combust. Inst., 35(3), pp. 3219–3227.

[16] Ghirardo, G., Boudy, F., and Bothien, M. R., 2018, "Amplitude Statistics Prediction in Thermoacoustics," J. Fluid Mech., 844, pp. 216–246.

[17] Brillouin, L., 1953, Wave Propagation in Periodic Structures: Electric Filters and Crystal Lattices, 2nd ed., Dover Publications, Mineola, NY, pp. 139–140.

[18] Munjal, M., 1987, Acoustics of Ducts and Mufflers, Wiley, Hoboken, NJ.

[19] Bender, C., and Orszag, S., 1978, Advanced Mathematical Methods for Scientists and Engineers, McGraw-Hill Book, New York.

[20] Miller, P., 2006, Applied Asymptotic Analysis, American Mathematical Society, Providence, RI.

[21] Stow, S. R., Dowling, A. P., and Hynes, T. P., 2002, "Reflection of Circumferential Modes in a Choked Nozzle," J. Fluid Mech., 467, pp. 215–239.

[22] Marble, F. E., and Candel, S., 1977, "Acoustic Disturbance From Gas Non-Uniformities Convected Through a Nozzle," J. Sound Vib., 55(2), pp. 225–243.

[23] Bauerheim, M., Duran, I., Livebardon, T., Wang, G., Moreau, S., and Poinsot, T., 2016, "Transmission and Reflection of Acoustic and Entropy Waves Through a Stator-Rotor Stage," J. Sound Vib., 374, pp. 260–278.

[24] Morgans, A. S., and Duran, I., 2016, "Entropy Noise: A Review of Theory, Progress and Challenges," Int. J. Spray Combust. Dyn., 8(4), pp. 285–298.

[25] Trefethen, L. N., 2000, Spectral Methods in MATLAB, Society for Industrial and Applied Mathematics, Philadelphia, PA.

[26] Krebs, W., Walz, G., Flohr, P., and Hoffmann, S., 2001, "Modal Analysis of Annular Combustors: Effect of Burner Impedance," ASME Paper No. GT2001-GT-0042.

[27] Morse, P. M., and Feshback, H., 1953, Methods of Theoretical Physics, Vol. 1, McGraw-Hill, New York.

[28] Schuermans, B., Bellucci, V., and Paschereit, C. O., 2003, "Thermoacoustic Modeling and Control of Multi Burner Combustion Systems," ASME Paper No. 2003-GT-38688.

[29] Gray, R. M., 2006, "Toeplitz and Circulant Matrices: A Review," Found. Trends Commun. Inf. Theory, 2(3), pp. 155–239.

[30] Moeck, J. P., Paul, M., and Paschereit, C. O., 2010, "Thermoacoustic Instabilities in an Annular Rijke Tube," ASME Paper No. GT2010-23577.

[31] Triantafyllou, M., and Triantafyllou, G., 1991, "Frequency Coalescence and Mode Localization Phenomena: A Geometric Theory," J. Sound Vib., 150(3), pp. 485–500.

[32] Schuermans, B., Polifke, W., and Paschereit, C. O., 1999, "Modeling Transfer Matrices of Premixed Flames and Comparison With Experimental Results," ASME Paper No. 99-GT-132.

[33] Goldmeer, J., Vandervort, C., and Sternberg, J., 2017, "New Capabilities and Developments in GE's DLN 2.6 Combustion Systems," Power-Gen International, Las Vegas, NV, Dec. 5–7, pp. 1–15.

[34] Sewell, J. B., and Sobieski, P. A., 2005, "Monitoring of Combustion Instabilities: Calpine's Experience," Combustion Instabilities in Gas Turbine Engines: Operational Experience, Fundamental Mechanisms, and Modeling (Progress in Astronautics and Aeronautics), T. C. Lieuwen and V. Yang, eds., American Institute of Aeronautics and Astronautics, Arlington, TX, pp. 147–162.

[35] Pierre, C., and Cha, D., 1989, "Strong Mode Localization in Nearly Periodic Disordered Structures," AIAA J., 27(2), pp. 227–241.